Theoretical Predictions of the Effects of Force Transmission by Desmin on Intersarcomere Dynamics

Gretchen A. Meyer,[†] Balázs Kiss,[‡] Samuel R. Ward,[§] David L. Morgan,[¶] Miklós S. Z. Kellermayer,[‡‖] and Richard L. Lieber[†*]

[†]Departments of Bioengineering and Orthopaedic Surgery, University of California, San Diego, and Veterans Affairs Medical Center, La Jolla, California; [‡]Department of Biophysics, University of Pécs, Faculty of Medicine Szigeti, Pécs, Hungary; [§]Department of Radiology, University of California, San Diego, California; [¶]Department of Electrical and Computer Systems Engineering, Monash University, Clayton, Victoria, Australia; and [‖]Department of Biophysics and Radiation Biology, Semmelweis University, Budapest, Hungary

ABSTRACT Desmin is an intermediate filament protein in skeletal muscle that forms a meshlike network around Z-disks. A model of a muscle fiber was developed to investigate the mechanical role of desmin. A two-dimensional mesh of viscoelastic sarcomere elements was connected laterally by elastic elements representing desmin. The equations of motion for each sarcomere boundary were evaluated at quasiequilibrium to determine sarcomere stresses and strains. Simulations of passive stretch and fixed-end contractions yielded values for sarcomere misalignment and stress in wild-type and desmin null fibers. Passive sarcomere misalignment increased nonlinearly with fiber strain in both wild-type and desmin null simulations and was significantly larger without desmin. During fixed-end contraction, desmin null simulations also demonstrated greater sarcomere misalignment and reduced stress production compared with wild-type. In simulations with only a fraction of wild-type desmin present, fixed-end stress increased as a function of desmin concentration and this relationship was influenced by the cellular location of the desmin filaments. This model suggests that desmin stabilizes Z-disks and enables greater stress production by providing a mechanical tether between adjacent myofibrils and to the extracellular matrix and that the significance of the tether is a function of its location within the cell.

INTRODUCTION

A skeletal muscle fiber is a three-dimensional meshwork of sarcomeres interconnected longitudinally and laterally by a network of cytoskeletal proteins. These proteins, including titin, α-actinin, dystrophin-associated proteins, and intermediate filaments, are fundamental to sustaining active and passive sarcomere loads. One fundamental component of the cytoskeleton is the intermediate filament protein desmin, which forms a network around the periphery of adjacent Z-disks, anchoring myofibrils to nuclei, mitochondria, and extracellular matrix (ECM) at the sarcolemma (1–3). The localization of desmin suggests that it may play an important role in muscle fiber force transmission. Specifically, it is proposed, desmin acts as a lateral mechanical link between Z-disks, providing stability to the fiber by maintaining sarcomere homogeneity and transmitting force radially (3,4). Desmin-related myopathies in humans have debilitating effects, highlighting the vital role desmin plays in the proper functioning of muscle.

Recent experiments involving the desmin null mouse have further defined the detrimental effects of desmin loss in skeletal muscle. Desmin null muscle fibers have decreased sarcomere connectivity, as measured by the stagger of radially adjacent myofibrillar Z-disks in electron micrographs of stretched extensor digitorum longus muscles (5). This result was later confirmed using immunofluorescence in stretched single fibers (6). In addition to these passive disparities, desmin null muscles develop lower fixed-end stress compared to wild-type muscles on the descending limb of the length-tension curve (7). It was surprising to find, however, that these muscles show less stress decline (injury) after eccentric contractions, even when correction is made for their smaller muscle size and initial stress production (7). Building on this study, desmin null fibers were transfected with a green-fluorescent-protein (GFP)-desmin fusion protein and functionally evaluated (8). Increasing GFP-desmin content was shown to attenuate Z-disk misalignment, increase fixed-end stress production, and increase injury as a logarithmic function of GFP-desmin content (8).

Although these studies have defined the functional consequences of desmin loss in muscle, the causative mechanism has yet to be described. High-resolution, real-time sarcomere array studies in intact muscle are currently not technically feasible, and thus, determining the role of desmin is an ideal problem to investigate using modeling.

Finite-element-type models of muscle fiber mechanics have already been developed (9,10) and have been used successfully to simulate experimental fiber behavior. Two models explicitly incorporate the intermediate filament lattice, but they are of small scale and include no connection to the ECM (11,12). Thus, the purpose of this study was to develop a two-dimensional finite-element model of a muscle fiber incorporating desmin as a linear elastic spring element connecting Z-disks laterally. This model was then used to simulate passive stretch and fixed-end contraction of desmin null and

Submitted April 21, 2009, and accepted for publication October 7, 2009.

*Correspondence: rlieber@ucsd.edu

Editor: Shin'ichi Ishiwata.

0006-3495/10/01/0258/9 $2.00

doi: 10.1016/j.bpj.2009.10.014

wild-type fibers and to predict the mechanical effect of desmin on sarcomere connectivity and fixed-end stress production.

METHODS

The sarcomere finite element

A finite-element model of a muscle fiber is constructed here as a repeating connection of sarcomere elements, similar to previous approaches (9,10). The mechanical equivalent of a sarcomere is represented as a viscoelastic structure similar to the three-element muscle model proposed by Hill (13). The contractile element (CE) represents the active force generated by myosin cross-bridges and is contiguous with an elastic element (SE) that represents their compliance (tendon is modeled explicitly here). A Maxwell viscoelastic unit (PVE) is connected in parallel with the CE and SE to model the passive tension and damping of titin and other proteins that extend longitudinally between Z-disks. The forces in the CE and PVE are nonlinear functions of sarcomere length (SL) and sarcomere shortening velocity (SL′) and are determined from scaled literature values for muscle fiber behavior (Table 1). The tension sustained by the SE is a linear function of extension (E).

The fiber is modeled as a two-dimensional array of sarcomere elements rigidly connected longitudinally to form myofibrils. Myofibrils are coupled laterally via desmin elastic elements (Fig. 1 *A*). Viscoelastic elements representing the ECM, including the sarcolemma, and the tendon are included in the model with properties estimated from the literature (Table 1). The ECM forms the lateral bounds of the array and the tendon caps at either end. The coupled, noninertial equations of motion are solved simultaneously at each nodal point.

Equations of motion

A free body diagram of the forces sustained by the sarcomere shows the active (*red*), elastic (*blue*), and damping (*green*) contributions to the nodal equations of motion (Fig. 1 *B*). The direction of the force in each element is indicated by arrows and the associated force (*upper case*) or element constant (*lower case*) is labeled. Calculating the sum of these forces at each node and setting the result equal to zero yields the nodal equations of motion in the longitudinal plane. Motion in the lateral plane is assumed to be negligible. Inertial forces are neglected in these equations due to the exceedingly small sarcomere mass. (Note that for inertial forces to be on the order of magnitude of viscous and elastic forces, the acceleration of a node would have to exceed 10^{12} μm/s^2, which is physiologically unreasonable (10).)

The contribution of the elastic force of a desmin filament to forces in the longitudinal plane is not a linear function of its extension even if the filament is linearly elastic, since the force acts obliquely to the plane. The relationship between the component of the filament extension ($f(x)$) and the net nodal displacement (x) in the longitudinal direction is given by

$$f(x) = x\left(1 - \frac{L}{\sqrt{L^2 + x^2}}\right), \tag{1}$$

where L is the unstretched filament length, which is exactly at rest, neither stretched nor slackened. When this function is incorporated into the desmin elastic terms, the equation of motion at node $x_{i,j}$ is given by

$$\begin{aligned} F_{i,j+1} - s_{i,j}\left(x_{i,j} - y_{i,j-1}\right) = {} & PT_{i,j} - PT_{i,j+1} + c_{i,j}\left(x'_{i,j} - x'_{i,j-1}\right) \\ & - c_{i,j+1}\left(x'_{i,j+1} - x'_{i,j}\right) - \ldots k_{i,j} f \\ & \times \left(x_{i-1,j} - x_{i,j}\right) - k_{i+1,j} f\left(x_{i+1,j} - x_{i,j}\right), \end{aligned} \tag{2}$$

where variables are as defined in Fig. 1 *B*. $k_{i,j}$ are the elastic spring constants of the desmin elements and $c_{i,j}$ are the passive sarcomere viscosity coefficients, both of which are constants. Location indices i and j are included simply to specify nodal position. The passive tension of the PVE elements is given by $PT_{i,j}$:

$$PT_{i,j} = p_{i,j}\exp\left(\frac{x_{i,j} - x_{i,j-1} - m}{\lambda}\right), \tag{3}$$

where m, λ, and $p_{i,j}$ are constants. The equation of motion at node $y_{i,j-1}$ is

$$F_{i,j} = s_{i,j}\left(x_{i,j} - y_{i,j-1}\right). \tag{4}$$

Note that this equation indicates that terms involving tension sustained by the SE in any equation (i.e., the lefthand side of Eq. 2) can be replaced by the force of the CE (i.e., the lefthand side of Eq. 4). Thus, the equations of motion are only evaluated at the $x_{i,j}$ nodes (Z-disks) and are of the form

$$\begin{aligned} F_{i,j+1} - F_{i,j} = {} & PT_{i,j} - PT_{i,j+1} + c_{i,j}\left(x'_{i,j} - x'_{i,j-1}\right) \\ & - c_{i,j+1}\left(x'_{i,j+1} - x'_{i,j}\right) - \ldots k_{i,j} f\left(x_{i-1,j} - x_{i,j}\right) \\ & - k_{i+1,j} f\left(x_{i+1,j} - x_{i,j}\right). \end{aligned} \tag{5}$$

TABLE 1 Model sensitivity analysis

Parameter	Reference	Value	Confidence	Sensitivity
Myofibril spacing	(30)	19 nm	3	0.0
Myofibril diameter	(6,31)	0.6 μm	4	**8.1**
Maximum contractile stress(of a sarcomere)	(15,32)	368 kPa	4	**8.1**
Sarcomere length range (end to center)	(9,19)	0.2 μm	3	0.3
Number of sarcomeres in series	(15,33)	200	2	0.6
Number of myofibrils in parallel	(6,15)	10	2	**7.7**
Passive tension exponential constant (m)	(6,9)	5.5 μm	2	0.3
Passive tension exponential constant (λ)	(6,9)	0.5	2	0.2
Length-tension curve (base width)	(15)	1.27–3.9 μm	4	**4.3**
Length-tension curve (peak width)	(15)	2.1–2.45 μm	4	0.0
Desmin elastic modulus		3.7 MPa	2	0.2
Passive viscosity coefficient	(18)	0.8 kN-s/m^2	2	1.0
Hill coefficients ($\frac{a}{P_0}$, $\frac{b}{V_{max}}$)	(15)	0.2	3	0.9
Maximum velocity in shortening	(15,34)	4 L/s	3	1.0
ECM passive stress at SL_{max}	(25–27)	743 kPa	**1**	1.9
Endomysium thickness	(25,27)	0.1 μm	3	1.9
Tendon elastic modulus	(35,36)	500 MPa	3	0.0

The 17 model parameters were based on experimental data taken from the reference(s) shown. Confidence in each parameter was estimated subjectively on a scale from 1–4. based on support for that value in the literature. Low confidence and high sensitivity values are in bold print.

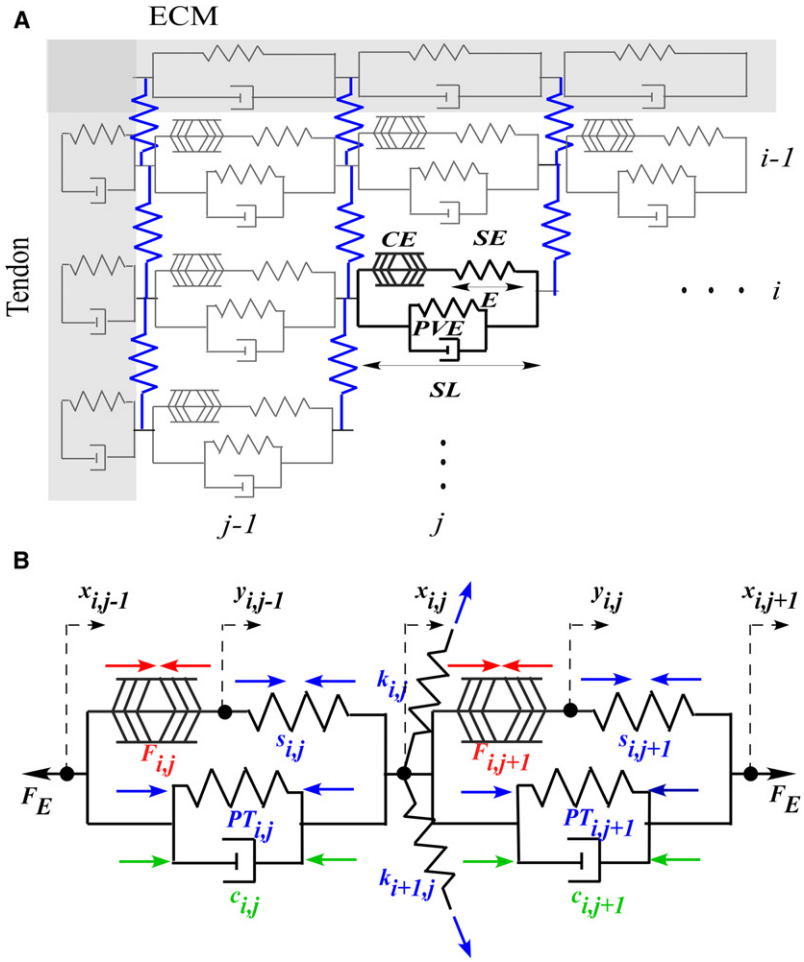

FIGURE 1 (*A*) Graphical representation of the finite-element muscle fiber array. (*B*) Free body diagram of two sarcomeres linked at a Z-disk. Viscoelastic sarcomere elements are linked longitudinally at Z-disk nodes to form myofibrils and laterally by desmin elastic filaments (*blue*) to form a two-dimensional fiber. ECM (and sarcolemma composite) elements form the upper and lower bounds of the array, whereas tendon elements define each end. The location of each element is indexed by its row (i) and column (j). The array continues to extend in the direction of increasing i and j until it meets another ECM/tendon junction. The contractile element (CE), the series elastic element (SE), the parallel viscoelastic element (PVE), the sarcomere length (SL), and the series spring extension (E) are labeled in the bold sarcomere. Forces involved in the calculation of the nodal equations of motion are illustrated by color-coded arrows (*red*, active; *blue*, elastic; and *green*, viscous). The parameters used in the calculation of these forces are labeled near their associated arrows, with forces listed in capital letters and constants in lower case. Dotted arrows and associated variables label the directions of positive nodal displacement from the initial position. Parameters and nodal displacements are also indexed with subscripts by their location in the finite-element array in the (row, column) format. Sign conventions are set assuming that $x_{i-1} < x_i < x_{i+1}$. Variables $x_{i,j}$ and $y_{i,j}$ are the displacements at the x and y nodes, respectively. F_E are the forces external to the sarcomeres pictured and $F_{i,j}$ is the contractile force in the CE of sarcomere (i,j). $PT_{i,j}$ is the passive tension developed in the PVE and $c_{i,j}$ is the damping constant of the PVE of the same sarcomere. Constant $s_{i,j}$ is the stiffness of the SE and $k_{i,j}$ is the stiffness of desmin.

The nodal equations of motion can be expressed in the general matrix form

$$Ax' + B\exp\left(\frac{(x-a)}{\lambda}\right) + Cf(x) = d, \qquad (6)$$

where x and x' are the displacement and velocity, respectively, of each node (Z-disk). Matrix A is the damping matrix and contains only the constants $c_{i,j}$. Matrices B and C contain the constants for PVE and desmin elasticity, respectively, whereas the vector d contains the forces of the contractile elements.

The complexity of this system of nonlinear differential equations is simplified by computing nodal velocities first, and then determining displacements from these velocities at discrete time steps, typically on the order of 0.01 ms. In this method, the x and $f(x)$ terms become constants that can be lumped into the contractile force term. Thus, the system is simplified to

$$Ax = b, \qquad (7)$$

where the variable of interest, x, is now velocity and b is a nonlinear function of nodal displacement.

Model parameters

The parameters used in the model equations were derived from 17 empirical measurements obtained from the literature, primarily from mouse muscle fibers (Table 1). Each parameter was assigned a subjective confidence level from 1 to 4 based on the number of corroborating studies, with 4 representing our opinion of an excellent assumption and 1 representing a questionable assumption. Then, a sensitivity analysis was performed for each model parameter to determine the relative change in force production resulting from a 10% parameter change. Sensitive parameters whose confidence is low represent more severe model limitations (however, all parameters in this model with sensitivities >4% had confidence levels of at least 2). These parameters were then incorporated into the relationships governing the behavior of the CE and PVE as discussed below.

The contractile element

The ability of a model sarcomere to generate contractile force was dependent on the degree of actin-myosin overlap in the manner originally described for single fibers by Gordon et al. (14). The model described here makes no attempt to model individual cross-bridge interactions, but instead uses the length-tension relationship measured by Edman et al. from mouse flexor digitorum brevis single fibers during fixed-end tetani (15). The piecewise linear curve fit has zero force at sarcomere lengths <1.27 μm, 0.72 times the maximum force at 1.68 μm, maximum force between 2.1 and 2.45 μm, and zero force above a sarcomere length of 3.9 μm (Fig. 2).

The force-generating capacity of a shortening sarcomere as a function of velocity was modeled using the classic Hill equation (13), whose constants were determined to be $b/V_{max} = a/P_0 = 0.2$ for mouse fast fibers (15). For lengthening sarcomeres, the force-velocity curve was assumed to have a slope equal to six times the shortening slope at very small velocities and a maximum force production of 1.8 P_0 (16) at maximum velocity, V_{max}. For simplicity, V_{max} is assumed to be constant in this model, although some variation with sarcomere length has been reported (17).

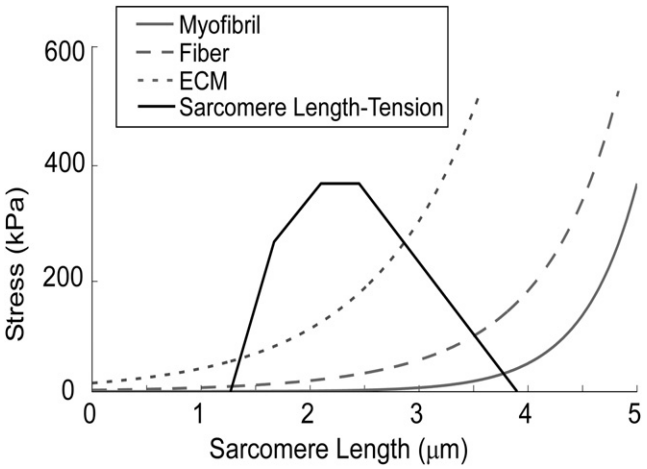

FIGURE 2 Passive stress of myofibril elements and ECM elements, and the average passive stress in the simulated fiber superimposed on the sarcomere length-tension diagram. Myofibril passive stress, ECM passive stress, and the sarcomere length-tension relationship were estimated from work by others (6,13,15, 25–27). The fiber average passive stress is calculated for a simulated fiber with 10 myofibrils laterally by summing the force contribution of each myofibril and the two ECM elements and dividing by the total cross-sectional area.

The parallel viscoelastic element

The passive-tension exponential constants used in this model were determined by fitting Eq. 3 to skinned mouse single-fiber stress/strain data (6) (Fig. 2). The viscosity coefficient of the sarcomere PVE was 0.8 kN s/m^2, as given by the mouse fast fiber data of Mutungi and Ranatunga (18).

Variation in sarcomere properties

Sarcomere elements in the model have identical properties except for their initial lengths (exponential variation) and passive tension (random variation) relationships, and each sarcomere is assumed to be symmetric. The initial sarcomere length distribution for a half-myofibril is defined by the equation

$$\mathrm{SL}_i = \mu_{\mathrm{SL}} - \delta_{\mathrm{SL}}\exp(-40i/N), \tag{8}$$

yielding end sarcomere lengths that are shorter than average and a sarcomere length distribution that is smooth along the length of the myofibril (19,20) (Fig. 3). The constants μ_{SL} and δ_{SL} are the mean sarcomere length and the sarcomere length range, respectively, of the distribution, i is the index of the current sarcomere, and N is the number of sarcomeres in a half-myofibril. This distribution is then mirrored at the center to create the myofibril distribution with shorter sarcomeres at each end.

Superimposed on this distribution is a 5% uniform random variation in the passive tension constant, λ (Fig. 3). This random component is intended to reflect the biological variation in passive load-bearing structures such as titin that contribute to sarcomere stiffness variation. This is one possible explanation for the variability in sarcomere lengths across the length of fibers and myofibrils observed experimentally (21,22).

Properties of the ECM and tendon

ECM and tendon elements are constructed of parallel viscoelastic and series elastic elements only and have no active element. In addition, the parameters of these elements are unique for the ECM and tendon compared to the sarcomeres. Initially, each ECM row is given an element length distribution identical to the initial sarcomere length distribution defined by Eq. 8 so that desmin elements initially are oriented laterally and have no longitudinal loading. Each myofibril is connected to two tendon elements, one on each end, and tendon elements do not interact with their lateral neighbors. Neither ECM nor tendon elements have random property variations.

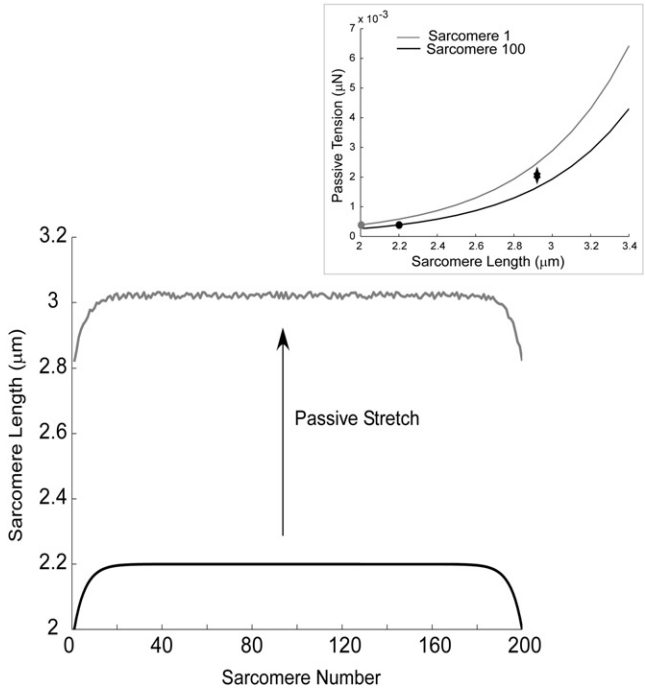

FIGURE 3 Sarcomere length distributions across the fiber length and depiction of initial passive tension (*inset*). The black trace is the sarcomere length distribution generated by Eq. 8, with a mean sarcomere length of 2.2 μm and a length range of 0.2 μm. The gray trace shows what happens to the distribution after passive stretch to a mean sarcomere length of 3 μm. The variation in sarcomere length is a result of the random variation in the passive tension coefficient, λ. (*Inset*) Passive tension curves for sarcomeres 1 and 100, where the curve for sarcomere 1 has been multiplied by a larger coefficient so that the passive tensions are equal for the two sarcomeres at their initial lengths (*dots* on *inset*).

Desmin stiffness

Desmin stiffness was calculated using atomic force microscopy measurements of isolated desmin filaments and fitting data to the wormlike chain model. The details of the desmin preparation and stiffness estimation can be found in the Supporting Material.

Simulations

All simulations used model fibers with 10 laterally connected myofibrils with 200 sarcomeres longitudinally. These dimensions were chosen for computational tractability. The computational routine determines the initial exponential sarcomere length distribution from a user-defined mean sarcomere length. This distribution is then used to calculate the passive tension relationship for each sarcomere by adjusting the constant $p_{i,j}$ from Eq. 3 such that all sarcomeres begin at the same initial passive tension and the fiber rests in static equilibrium. This adjustment is illustrated in the inset of Fig. 3, where the curve for sarcomere 1 is adjusted by increasing its $p_{i,j}$ compared to sarcomere 100 so that the two sarcomeres at different initial lengths have the same passive tension. The isometric force producing capacity (P_0) of each contractile element is calculated using the "sarcomere" length-tension curve (Fig. 2). An activation ramp is then imposed on the fiber using

$$P = \left(\frac{t}{0.005 + t}\right)P_{\mathrm{o}}, \tag{9}$$

where P is the amount of force the sarcomere can generate at time t (s), to ensure that sarcomeres don't switch from passive to active instantaneously. The contractile element force and velocity are then computed from the equations of motion and the force-velocity curve. The sarcomere length distribution is updated by multiplying contraction velocity by a discrete time step, and the computation is then repeated under the new conditions. Thus, the routine computes the strain map and force production of the fiber over time. Stress production is calculated by dividing the force by the average cross-sectional area of a mouse EDL myofibril multiplied by the number of myofibrils in parallel.

Passive stretch was performed on ten simulated fibers, each with a unique variation in sarcomere properties (length and passive tension), by constraining fiber ends to move with a constant velocity of 0.085 mm/s and allowing stretch from a mean sarcomere length of 2.2 μm to 5 μm (strain = 1.27). Data are presented as the mean and standard deviations of these 10 fibers. Z-disk stagger was determined by computing the absolute difference between the positions of laterally adjacent nodes over the length of the fiber and averaging these values at each Z-disk (column). Mean Z-disk stagger was determined every ~5% strain by averaging Z-disk stagger over the length of the fiber.

Fixed-end contraction was also simulated with 10 fibers. Immediately before activation, sarcomeres are simulated to stretch from a mean sarcomere length of 2.2 μm to 3 μm as described above. This was intended to provide a variation in sarcomere lengths at 3 μm and does not qualitatively affect the simulation results. Sarcomeres were then activated for 2.5 s. Measurements of Z-disk stagger were made, as described above, in increments of ~100 ms, and fixed-end stress production was computed as the maximum stress achieved during the simulation. All simulations were written and executed in MATLAB (The MathWorks, Natick, MA).

RESULTS

Passive stretch

To investigate the effect of strain on sarcomere alignment, passive stretch of 10 wild-type and 10 desmin null fibers was simulated, differing only in the random component of their initial passive tension parameter. Desmin null fibers had significantly greater mean Z-disk stagger than wild-type at sarcomere lengths >3 μm (Fig. 4 *A*). Both the magnitude and the discrepancy in mean Z-disk stagger between desmin null and wild-type fibers increased nonlinearly as a function of strain. To find any localization of high Z-disk misalignment, the stagger of each Z-disk along the fiber length was measured. Z-disk stagger was significantly higher for desmin null fibers along the length of the fiber, with the exception of the fiber ends, which were constrained by the tendon to have near-zero stagger (Fig. 4 *B*). The midsection of the fiber is predicted to have the highest Z-disk misalignment.

Fixed-end contraction

Fixed-end contractions of 10 wild-type and 10 desmin null fibers were simulated with the same parameters used for the passive stretch simulations. Intersarcomere dynamics, similar to those observed using the model of Morgan et al. (9), demonstrated that end sarcomeres rapidly shortened, whereas center sarcomeres lengthened during contraction (Fig. 5). Similar to passive stretch simulations, mean Z-disk stagger measurements showed significantly greater misalignment for desmin null fibers over the contraction, and this discrepancy increased as a function of time (Fig. 6 *A*). In addition, the stagger at the majority of Z-disks along the fiber was significantly higher for desmin null than for wild-type fibers (Fig. 6 *B*). Again, the largest misalignment occurred in the fiber midsection.

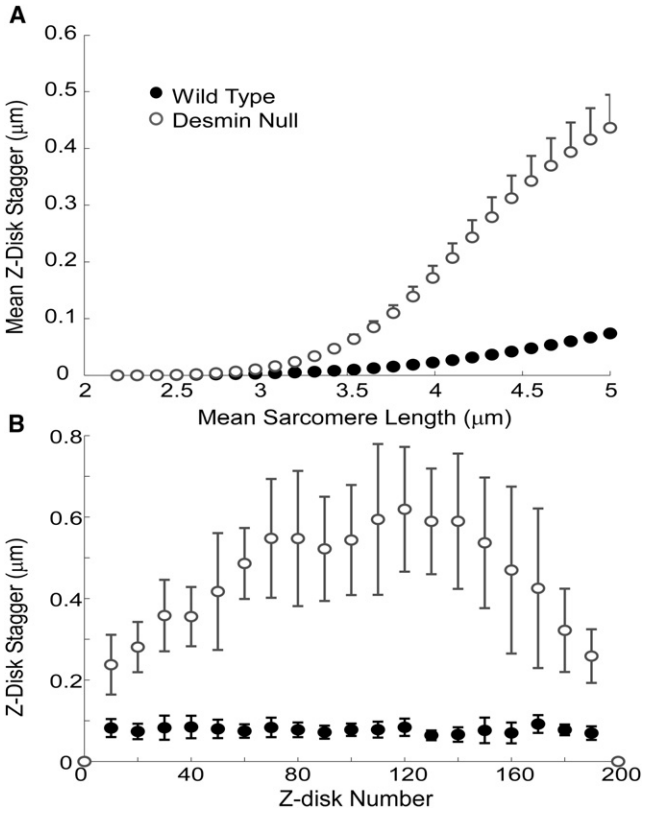

FIGURE 4 (*A*) Mean Z-disk stagger as a function of sarcomere length over the course of a passive stretch. (*B*) Measurements of stagger at every 10th Z-disk over the length of the fiber at a sarcomere length of 5 μm. Data points are the mean value from 10 runs in each group, with a different random variation in the passive tension constant used for each run, and error bars are the standard deviations. Desmin null fibers have a significantly higher mean Z-disk stagger than wild-type at all sarcomere lengths >3 μm and at all Z-disks except for the fiber ends, which are constrained. Some error bars are small and are obscured by the data marker.

Stress production was also examined during fixed-end contractions. Fixed-end stress production was reduced by ~20% in the simulated desmin null fiber compared with wild-type (Fig. 7). To investigate the role desmin localization plays in fixed-end stress development, desmin links were applied to 1, 5, 10, 25, 50, and 90% of the possible Z-disk connections, using one of three spatial arrangements: 1), randomly across the fiber; 2), preferentially to the ECM; or 3), preferentially away from the ECM. To select preferential arrangement, each desmin link was assigned a number based on its position in the fiber array. The numbers were then arranged into a vector of length 11 fibers × 199 sarcomeres, with either the ''peripheral'' or ''central'' numbers in the center. Then, an algorithm was used which drew

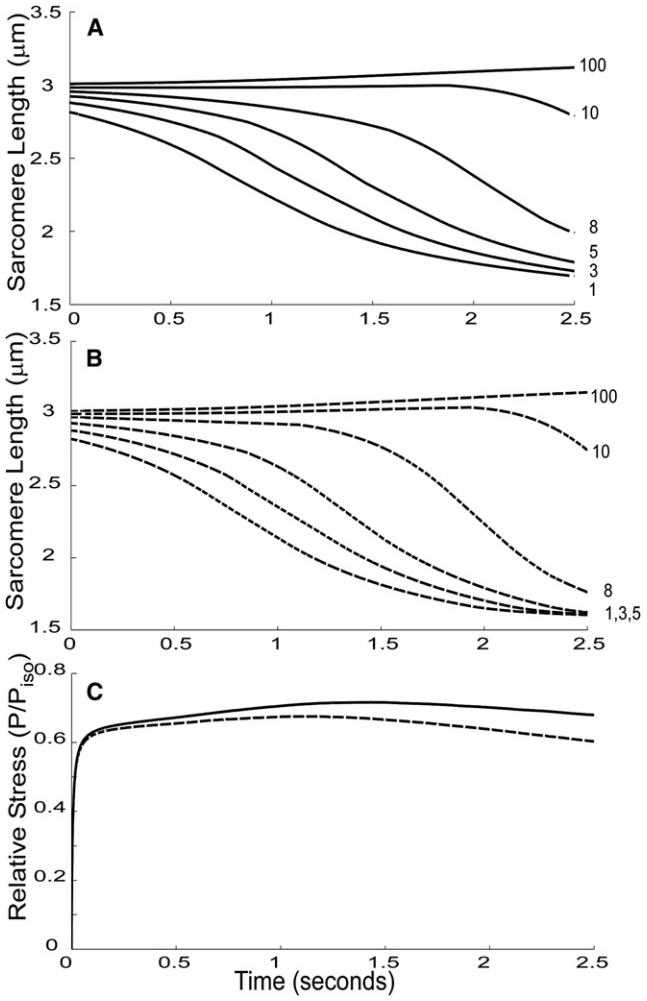

FIGURE 5 Length traces over time of a representative run for selected sarcomeres from wild-type (*A*) and desmin null (*B*) fibers and the overall normalized force traces (*C*) during simulated fiber fixed-end contraction. Solid lines correspond to wild-type simulations and dotted lines to desmin null. Sarcomere numbers are increasing along the length of the fiber, and each number is shown adjacent to the corresponding trace on the right side of the plot. This plot shows that end sarcomeres shorten significantly over the contraction period, whereas center sarcomeres lengthen more slowly and continuously. Note that end sarcomeres in the desmin null traces (*B*) are shorter than in the wild-type (*A*), and their corresponding force is lower (*C*). Compare with simulations reported previously (Figs. 4 *A* and 5 in Morgan et al. (9)).

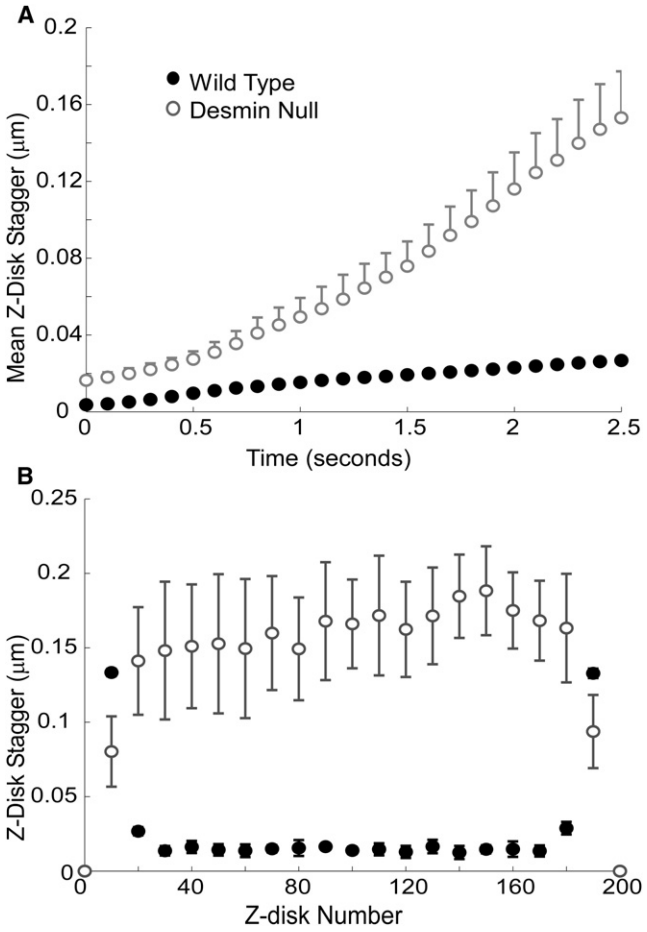

FIGURE 6 (*A*) Z-disk stagger as a function of the time course of simulated fixed-end contraction. (*B*) Measurements of stagger at every 10th Z-disk over the length of the fiber at 2.5 s. Mean Z-disk stagger is significantly higher for desmin null fibers than for wild-type at all time points and increases nonlinearly as a function of time. Z-disk stagger and hence differences in stagger between wild-type and desmin null fibers are small at the fiber ends due to the abrupt force drop modeled in the contractile element, with shortening beyond 1.68 μm sarcomere length and the limited opportunity for sarcomere length variations to add up to large staggers due to the proximity to the tendon. Z-disk staggers are on the same order as those seen during passive stretch.

pseudorandom numbers from a normal distribution with a mean at the center of the vector and a standard deviation of 200. This number was used to index the vector, selecting a specific desmin link. The relationship between desmin content and fixed-end stress production showed a different degree of nonlinearity for each case considered.

Restoring 1% of the desmin content in the desmin null fiber at the ECM attenuated 40% of the fixed-end stress-producing deficit. Restoring 1% of the desmin randomly attenuated the deficit by 10%, whereas away from the ECM, 1% desmin did not significantly change the fixed-end stress. When 50% of the desmin content was restored either near the ECM or randomly, the stress-producing deficit was reduced by 97% or 88%, respectively; however, when desmin was localized away from the ECM, this degree of stress restoration is not seen until the desmin concentration is at 90%. When 90% of the desmin was restored either to the ECM or randomly, the stress production was not significantly different from that seen in the wild-type fiber (Fig. 7).

DISCUSSION

This model was developed to isolate the mechanical contributions of desmin to sarcomere movement during passive stretch and fixed-end contraction. We based our assumptions on relationships that have been demonstrated in single fibers,

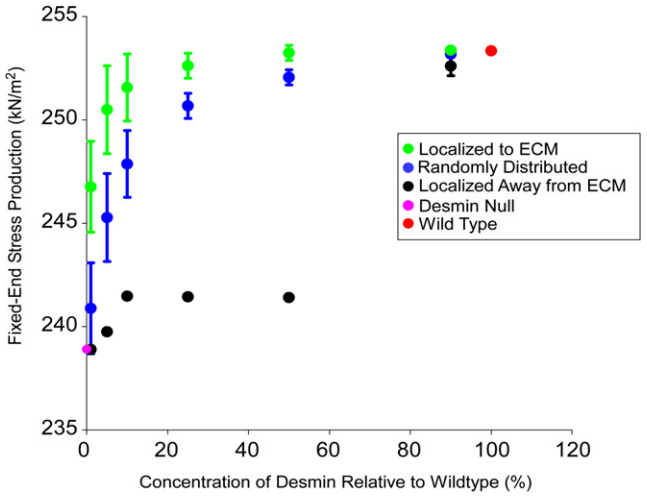

FIGURE 7 Plot of the maximum fixed-end stress production during simulated fixed-end contraction of fibers with varying concentrations and localizations of desmin. Stress production is greater when desmin is preferentially localized to the fiber membrane (*green*) than when it is distributed randomly (*blue*) or preferentially localized away from the fiber membrane (*black*). Each data point represents the mean of 10 simulations under its color-coded condition, and error bars are standard deviations.

then scaled to the sarcomere level, an approach validated by previous investigators (9,10). The novel aspect of this model is that it explicitly incorporates desmin intermediate filament elements into the finite-element mesh at locations, and in orientations, that they appear to occupy based on structural data (3,4). In addition, we measured material properties of isolated desmin filaments and incorporated them into the model, thus increasing the model's predictive potential.

The novel predictions of the model are that 1), desmin modulates intersarcomere dynamics during passive stretch and fixed-end contraction; 2), by anchoring to the ECM, and thus restricting sarcomere shortening, desmin enables the fiber to produce more active stress; and 3), the magnitude of this effect is dependent on the localization of desmin, with desmin near the ECM having the most influence on stress production. Results suggest that the experimentally observed increase in sarcomere misalignment during passive stretch (5,6), decrease in fixed-end stress production (7), and, as discussed later, relationship between desmin concentration and injury (8) may be explained, at least in part, by the loss of desmin between Z-disks and the ECM.

Desmin null simulated fibers were shown to have significantly higher Z-disk misalignment in comparison with wild-type fibers during passive stretch at nearly all strains and across the majority of the fiber length (Fig. 4). These results are consistent with previous demonstrations of increased ''Z-disk displacement'' (our ''stagger'') observed in electron micrographs (5) and increased Z-disk variance using confocal microscopy (6). The magnitude of ''Z-disk displacement'' measured was in the range of 0–0.5 μm, which is consistent with model predictions. The results also agree with the observation that the difference between wild-type and desmin null ''displacements'', as well as the magnitudes of each in passive muscle, increase with increasing strain (5,6).

Agreement between model predictions of misalignment during passive stretch and experimental observations supports the idea that desmin acts to mechanically couple sarcomeres, thereby restricting longitudinal shear, the movement of a myofibril past its neighbor. The predicted attenuation of shear is primarily a function of the sarcomeric variation in the passive tension parameter at long length and the elastic modulus of desmin. An overestimate of either parameter would result in an overprediction of the increase in desmin null sarcomere misalignment over that of wild-type. The estimated random variation in the passive tension parameter resulted in a 1% predicted variation in sarcomere length after passive stretch from a mean sarcomere length of 2.2 μm to 5 μm. Based on experimental data that cite the variation in sarcomere length along a fiber to be between 2 and 11%, the modeled passive tension parameter variation is likely conservative (14,22,23).

The elastic modulus used for desmin was determined using the wormlike chain model. It is possible that if the filaments are stretched longitudinally with relatively large forces, deviations will occur from the theoretically predicted entropic chain behavior. Recent studies by Kreplak et al. (24) in which the center of an isolated desmin filament was stretched perpendicular to the long axis revealed a desmin modulus between 10 and 15 MPa, which is considerably larger than the value computed here. Their experiment is subject to its own assumptions and limitations, but it is reasonable to assume that the modulus value used in this model is conservative. In addition, it is possible that each lateral connection is composed of more than just the one filament modeled here. In the model, incorporating more filaments would be equivalent to increasing the stiffness of the desmin spring. The one-filament link is used here to be a limiting conservative case, as an increase in the stiffness of desmin increases its effect on sarcomere alignment and stress production.

No experimental data are available that compare Z-disk alignment between wild-type and desmin null fibers during fixed-end contraction, but we predict from these simulations that Z-disk misalignment would be higher in desmin null compared with wild-type fibers (Fig. 6).

By coupling sarcomeres laterally and anchoring them to the ECM, desmin serves as a mechanism to prevent large length discrepancies between laterally adjacent sarcomeres. If a sarcomere were to attempt to shorten faster than its neighbors, desmin filaments would transmit a portion of this force to adjacent sarcomeres or to the ECM, preventing shortening of the original sarcomere until its neighbors could ''catch up''. Thus, the desmin intermediate-filament network behaves as an intersarcomere stiffness, preventing sharp divisions in length between sarcomere populations. In fact, comparison of a simulation run by Morgan et al. (9,20) that lacked intersarcomere stiffness to one including

intersarcomere stiffness show differences similar to those seen in comparing Fig. 5, *A* and *B,* in this article. The initial stress rise is similar, but the peak is somewhat lower and the decline after the peak is faster. This model suggests, then, a possible mechanism for intersarcomere stiffness that warrants a more in-depth exploration.

Stress production during fixed-end contraction was predicted by the model to be on average 20% lower for desmin null fibers compared to wild-type fibers (Fig. 7). This result is consistent with experimental data indicating that on the descending limb of the length-tension curve, desmin null muscles produce 10–20% lower fixed-end stress compared to wild-type muscles (7). The mechanistic basis for this prediction is that desmin behaves as a tether, limiting the longitudinal variation in sarcomere length. In the absence of this tether, end sarcomeres, which begin on the descending limb of the length-tension curve, are allowed to shorten more freely and cross the plateau onto the ascending limb.

The predicted decrease in fixed-end stress production in desmin null fibers is a function of the modulus of desmin, the properties of the ECM elements, the initial sarcomere lengths, and the dimensions of the sarcomere array. An overestimate of the modulus of desmin would result in a tighter link to adjacent myofibrils and to the ECM, which would increase the simulated difference in fixed-end stress between desmin null and wild-type fibers. However, as discussed previously, we believe our value to be conservative. An overestimate of the ECM element modulus would also result in an overprediction of the mechanical contribution of desmin to stress production. The modulus used here for the sarcolemma and ECM composite is below values found in the literature (25–27), so we believe this value to be conservative as well.

All simulations presented here were activated at a mean sarcomere length of 3 μm, which is on the descending limb of the length-tension curve. At these lengths, intersarcomere dynamics play a large role in stress generation, as demonstrated by the rapid shortening of end sarcomeres and the gradual lengthening of central sarcomeres (9). The predicted drop in fixed-end stress production for desmin null fibers is a direct consequence of this phenomenon, as end-sarcomere velocity is unrestrained and sarcomeres cross onto the ascending limb of the length-tension curve. Simulations run with mean sarcomere lengths beginning on the plateau or ascending limb show little to no difference in stress production between wild-type and desmin null models. This is consistent with published results by other groups, who have reported no significant stress difference between wild-type and desmin null muscles at optimal length (28,29).

The dimensions of the sarcomere array were chosen based on computational tractability and are only about one-tenth the size of a mouse fiber in the lateral and longitudinal directions. In addition, the model only includes sarcomeres in two dimensions, whereas myofibrils in a real fiber are arranged in a three-dimensional hexagonal close-packing arrangement. Increasing the model dimensions laterally increases the distance between the central sarcomeres and the stiffer ECM, decreasing the desmin-mediated influence it has over them. However, explorative model runs at half and twice the current dimensions have shown only changes in the quantitative effects of desmin and have the same qualitative effect. We believe that further increasing the model to realistic dimensions would have the same result: increased stagger and decreased stress production for the desmin null over the wild-type case, with the same dependence on desmin location. In addition, although central sarcomeres will be further removed from the ECM in a three-dimensional model of correct dimensions, they will also be connected to more neighboring myofibrils, which will in turn interconnect with even more neighbors, eventually binding the ECM >300 times/Z-line. Thus, expanding the scale to three dimensions would serve to dramatically increase the desmin-mediated influence of the ECM, making our two-dimensional model a conservative case.

In wild-type model fibers, end-sarcomere shortening is restrained by the ECM only because desmin transmits force between it and adjacent Z-disks. In the fiber center, desmin acts to restrain relative stagger between laterally adjacent sarcomeres, but does not provide the same anchoring effect as it does at the ECM. As expected, the model then predicts that if desmin links are restored preferentially at the ECM, fixed-end stress production is increased compared to the case where they are restored in the interior of the fiber. As more elements are restored to the ECM, stress increases dramatically until all are present (~20% desmin concentration in this model); then stress production begins to level off as desmin concentration increases to 100%. This is an interesting result in light of recent findings by Palmisano et al. (8) that injury to desmin transfected fibers increases with desmin content in a similar logarithmic fashion. This data may indicate that transfected desmin localizes preferentially to the membrane to maximize the stability it can provide to the fiber.

If a larger sarcomere array was used in these simulations, the ratio of ECM desmin links to central fiber links would decrease, making it less likely that an ECM link would be chosen at random. This would then cause the randomly distributed desmin prediction (Fig. 7, *blue curve*) to more closely resemble the prediction where desmin is selected away from the ECM (Fig. 7, *black curve*), strengthening the case for preferential desmin localization. Future experimental studies are required to investigate whether desmin localization plays a role in stress generation during fixed-end contractions.

SUPPORTING MATERIAL

Details of the desmin preparation and stiffness estimation and two figures are available at http://www.biophysj.org/biophysj/supplemental/S0006-3495(09)01621-X.

We thank Sameer Shah and Alireza Amirkhizi for their helpful comments and insights.

We gratefully acknowledge support from the National Institutes of Health (grant AR40050) and the Department of Veterans Affairs.

REFERENCES

1. Granger, B. L., and E. Lazarides. 1979. Desmin and vimentin coexist at the periphery of the myofibril Z disc. *Cell.* 18:1053–1063.
2. Paulin, D., and Z. Li. 2004. Desmin: a major intermediate filament protein essential for the structural integrity and function of muscle. *Exp. Cell Res.* 301:1–7.
3. Wang, K., and R. Ramirez-Mitchell. 1983. A network of transverse and longitudinal intermediate filaments is associated with sarcomeres of adult vertebrate skeletal muscle. *J. Cell Biol.* 96:562–570.
4. Lazarides, E. 1980. Intermediate filaments as mechanical integrators of cellular space. *Nature.* 283:249–256.
5. Shah, S. B., F. C. Su, …, R. L. Lieber. 2002. Evidence for increased myofibrillar mobility in desmin-null mouse skeletal muscle. *J. Exp. Biol.* 205:321–325.
6. Shah, S. B., J. Davis, …, R. L. Lieber. 2004. Structural and functional roles of desmin in mouse skeletal muscle during passive deformation. *Biophys. J.* 86:2993–3008.
7. Sam, M., S. Shah, …, R. L. Lieber. 2000. Desmin knockout muscles generate lower stress and are less vulnerable to injury compared with wild-type muscles. *Am. J. Physiol.* 279:C1116–C1122.
8. Palmisano, M. G., S. N. Bremner, …, R. L. Lieber. 2007. Rescue of mechanical function in desmin knockout muscles by plasmid transfection. *In* Annual Meeting of the Orthopaedic Research Society, San Diego, CA. Paper No. 33.
9. Morgan, D. L., S. Mochon, and F. J. Julian. 1982. A quantitative model of intersarcomere dynamics during fixed-end contractions of single frog muscle fibers. *Biophys. J.* 39:189–196.
10. Denoth, J., E. Stüssi, …, G. Danuser. 2002. Single muscle fiber contraction is dictated by inter-sarcomere dynamics. *J. Theor. Biol.* 216: 101–122.
11. Anderson, J., Z. Li, and F. Goubel. 2002. Models of skeletal muscle to explain the increase in passive stiffness in desmin knockout muscle. *J. Biomech.* 35:1315–1324.
12. Telley, I. A., J. Denoth, and K. W. Ranatunga. 2003. Inter-sarcomere dynamics in muscle fibres. A neglected subject? *Adv. Exp. Med. Biol.* 538:481–500; discussion 500.
13. Hill, A. V. 1938. The heat of shortening and the dynamic constants of muscle. *Proc. R. Soc. Lond. B. Biol. Sci.* 126:136–195.
14. Gordon, A. M., A. F. Huxley, and F. J. Julian. 1966. The variation in isometric tension with sarcomere length in vertebrate muscle fibres. *J. Physiol.* 184:170–192.
15. Edman, K. A. 2005. Contractile properties of mouse single muscle fibers, a comparison with amphibian muscle fibers. *J. Exp. Biol.* 208:1905–1913.
16. Katz, B. 1939. The relation between force and speed in muscular contraction. *J. Physiol.* 96:45–64.
17. Edman, K. A. 1979. The velocity of unloaded shortening and its relation to sarcomere length and isometric force in vertebrate muscle fibres. *J. Physiol.* 291:143–159.
18. Mutungi, G., and K. W. Ranatunga. 1996. The viscous, viscoelastic and elastic characteristics of resting fast and slow mammalian (rat) muscle fibres. *J. Physiol.* 496:827–836.
19. Huxley, A. F., and L. D. Peachey. 1961. The maximum length for contraction in vertebrate straiated muscle. *J. Physiol.* 156:150–165.
20. Morgan, D. L. 1990. New insights into the behavior of muscle during active lengthening. *Biophys. J.* 57:209–221.
21. Edman, K. A., and F. W. Flitney. 1982. Laser diffraction studies of sarcomere dynamics during "isometric" relaxation in isolated muscle fibres of the frog. *J. Physiol.* 329:1–20.
22. Telley, I. A., J. Denoth, …, R. Stehle. 2006. Half-sarcomere dynamics in myofibrils during activation and relaxation studied by tracking fluorescent markers. *Biophys. J.* 90:514–530.
23. Burton, K., W. N. Zagotta, and R. J. Baskin. 1989. Sarcomere length behaviour along single frog muscle fibres at different lengths during isometric tetani. *J. Muscle Res. Cell Motil.* 10:67–84.
24. Kreplak, L., H. Herrmann, and U. Aebi. 2008. Tensile properties of single desmin intermediate filaments. *Biophys. J.* 94:2790–2799.
25. Rapoport, S. I. 1972. Mechanical properties of the sarcolemma and myoplasm in frog muscle as a function of sarcomere length. *J. Gen. Physiol.* 59:559–585.
26. Fields, R. W., and J. J. Faber. 1970. Biophysical analysis of the mechanical properties of the sarcolemma. *Can. J. Physiol. Pharmacol.* 48: 394–404.
27. Tidball, J. G. 1986. Energy stored and dissipated in skeletal muscle basement membranes during sinusoidal oscillations. *Biophys. J.* 50:1127–1138.
28. Balogh, J., Z. Li, …, A. Arner. 2003. Lower active force generation and improved fatigue resistance in skeletal muscle from desmin deficient mice. *J. Muscle Res. Cell Motil.* 24:453–459.
29. Wieneke, S., R. Stehle, …, H. Jockusch. 2000. Generation of tension by skinned fibers and intact skeletal muscles from desmin-deficient mice. *Biochem. Biophys. Res. Commun.* 278:419–425.
30. Goldspink, G. 1971. Changes in striated muscle fibres during contraction and growth with particular reference to myofibril splitting. *J. Cell Sci.* 9:123–137.
31. Goldspink, G. 1970. The proliferation of myofibrils during muscle fibre growth. *J. Cell Sci.* 6:593–603.
32. González, E., M. L. Messi, and O. Delbono. 2000. The specific force of single intact extensor digitorum longus and soleus mouse muscle fibers declines with aging. *J. Membr. Biol.* 178:175–183.
33. Felder, A., S. R. Ward, and R. L. Lieber. 2005. Sarcomere length measurement permits high resolution normalization of muscle fiber length in architectural studies. *J. Exp. Biol.* 208:3275–3279.
34. Barclay, C. J., and G. A. Lichtwark. 2007. The mechanics of mouse skeletal muscle when shortening during relaxation. *J. Biomech.* 40:3121–3129.
35. Wu, J. J. 2006. Quantitative constitutive behaviour and viscoelastic properties of fresh flexor tendons. *Int. J. Artif. Organs.* 29:852–857.
36. Bensamoun, S. F., T. Tsubone, …, P. C. Amadio. 2006. Age-dependent changes in the mechanical properties of tail tendons in TGF-β inducible early gene-1 knockout mice. *J. Appl. Physiol.* 101:1419–1424.